Chapter 11
Hydrogen and Calorimetry: Case Studies

Simona Bennici and Aline Auroux

Abstract In this chapter the use of calorimetric data is shown to be of primary interest for the determination of the reaction/diffusion and reaction/absorption mechanisms involved in hydrogen storage or hydrogen production reactions. Examples of calorimetric measurements (alone or coupled to volumetric devices working at atmospheric or high pressure) and thermal analysis experiments applied to different hydrogen storage systems are reported. In particular, applications of calorimetric tools to the study of irreversible and reversible hydrogen storage systems are detailed, such as borohydrides hydrolysis and hydrogen desorption from magnesium hydrides.

11.1 Introduction

Hydrogen as energy vector is one of the most promising approaches to the challenges posed by global warming, and hydrogen-based fuel cell technologies are expected to become one of the most prevalent energy sources in the near future [1, 2].

Now that technologies to use hydrogen as a clean fuel are readily available, like the Proton Exchange Membrane Fuel Cell (PEMFC), and can be developed at an industrial scale, research mainly focuses on the barrier of development which is hydrogen storage for delayed use. In fact, if nowadays the H_2 production methods are well known and controlled, the storage and transportation of the fuel remain major obstacles to its use [3].

During the last decade a lot of research effort has been put into the development of suitable and safe technologies for hydrogen storage, such as materials for high-pressure cylinders, liquefaction processes, hydrogen adsorption materials, and metal hydrides [4, 5], adaptable to a wide range of applications from stationary and automotive to portable devices. Although H_2 adsorption capacities have recently been

S. Bennici (✉) · A. Auroux

Institut de recherches sur la catalyse et l'environnement de Lyon, UMR5256,
CNRS-Université Lyon1, 2 avenue Einstein, 69626 Villeurbanne, France
e-mail: simona.bennici@ircelyon.univ-lyon1.fr

brought up to values near 6–8 wt%, this storage method requires a high pressure and low temperature.

Portable applications in particular require the implementation of H_2 technologies in the short term, due to a rapidly growing market and ever increasing energy demand. In this case, conception of a H_2 storage/generation system operating under ambient conditions is a primary requirement. The ultra-pure hydrogen produced by hydrolysis of metal borohydrides, possessing the right humidity level, can be directly used in PEM fuel cells, which represents a very interesting alternative to lithium-ion battery. At parity of mass, PEM based systems are 5–6 times more performing than lithium batteries [6]. Moreover, chemical hydrides have an excellent potential for high energy density storage at room temperature and ambient pressure [4, 5, 7].

To enable the commercialisation of fuel cells and hydrogen technologies, governmental institutions worldwide are working to identify the most promising hydrogen storage systems in order to promote the future R&D activities [7–9]. U.S Department of Energy in particular has excluded the use of $NaBH_4$ for on-board vehicle hydrogen storage due to its drawbacks in terms of exothermic reaction and formation of very stable dehydrogenated products. The high energy consumption required for the regeneration of these stable products back into hydrogen-containing fuel contributes to an inefficient overall energy balance [10]. Despite this, $NaBH_4$ remains a promising candidate for mobile, portable and stationary isolated site applications in which the targets are less demanding than for automotive applications and the final product price can be relatively high [11].

An appropriate catalyst is necessary to carry out the hydrolysis reaction at a high rate. Noble metal based catalysts were initially developed and studied for this purpose [5, 12–15], but the high cost of these materials associated with the low supply available shifted the focus of research towards cheaper catalytic materials. In fact, non-noble metals that form boride compounds such as Ni-B or Co-B alloys are efficient and low-cost catalysts for this reaction [6, 8, 11, 12, 16–19].

Besides borohydrides, solid state complex hydrides [20] such as magnesium, sodium, and lithium aluminium hydrides [21, 22], lithium amides [23], and their combination with MgH_2 [24, 25] have also proven to be potential candidates, in this case for reversible hydrogen storage. The goal of the recent research is to overcome the kinetic limitation and/or thermodynamic stability of Mg-based hydrogen storage materials adding additives and catalysts to these mixtures [26, 27].

A third class of materials potentially useful in hydrogen storage is nanostructured materials (i.e. carbon nanofibers, carbon nanotubes, zeolites, clathrate hydrates, metal-organic frameworks (MOFs)) that by virtue of their large surface-to-volume ratios can adsorb considerable amounts of hydrogen in the molecular state via weak molecular-surfacic interactions (physisorption) [4, 28–31]. For these materials the main challenge is to find ways by which they can be engineered to store reversibly high quantity of hydrogen close to room temperature.

For all the cited hydrogen storage systems, a precise determination of the heat of reaction is needed for an industrially applicable system design and evaluation of feasibility. The measurement of the heat evolved during a catalytic reaction or a

hydrogen desorption process is important from both the practical and fundamental points of view.

Firstly it is an essential tool for the assessment of thermal risks related to the performance of the reacting system at industrial scale (i.e. the capability of a system to enter into a runaway reaction). This type of safety data is particularly important for reactions like hydrogen generation by hydrolysis of borohydrides, where the rapid increase in temperature may result in a sharp pressure increase. Secondly the thermodynamic data are of primary interest for the determination of the reaction/diffusion and reaction/absorption mechanisms.

Therefore, calorimetry and thermal analysis techniques alone or preferentially combined to volumetric systems play a fundamental role in the study of hydrogen storage materials and related phenomena.

11.2 First Case Study: Irreversible H_2 Storage (Borohydrides)

The potential applications of sodium borohydride have been widely studied and most of the research efforts and industrial devices developed up to now are based on the catalyzed hydrolysis of sodium borohydride solutions (stabilized with NaOH) [32], Eq. 11.1.

$$NaBH_4(aq) + 4H_2O(l) \rightarrow NaB(OH)_4(aq) + 4H_2(g) \qquad (11.1)$$
$$\Delta_r H^\circ = -250.5 \, kJ.mol_{NaBH4}{}^{-1}$$
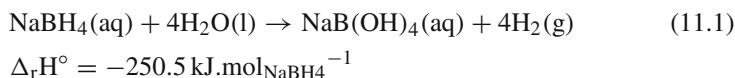
Sodium borohydride hydrolysis in aqueous solution can be represented in terms of the overall stoichiometric equation (Eq. 11.1) where $NaBH_4$ reacts with 4 molecules of water to produce 4 molecules of H_2 [33]. Although the reaction of $NaBH_4$ hydrolysis has been studied since the discovery of sodium borohydride by Stock in 1933 [34], the theoretical, calculated energy of the reaction is often cited in an incompatible manner to the application, and real experimental data are very scarce [35–38]. The thermodynamic features of the catalyzed hydrolysis in fact are not yet well understood, as the evolved energy depends on the physical state and the hydration degrees of borohydride and metaborate and on-side reactions.

Calorimetric techniques, and liquid phase calorimetry in particular, are promising methods to study catalytic reactions [39]. Notably, the use of a differential reaction calorimeter (DRC) makes it possible to determine the most important thermodynamic data such as the heat of reaction and heat capacity of the system [40–42].

11.2.1 Hydrolysis of $NaBH_4$ Stabilized Solutions

The study of Garron et al. [43] is one of the first investigations by liquid-phase calorimetry of the mechanism of hydrogen generation by hydrolysis of sodium

borohydride catalysed by Co_2B nanoparticles generated in situ. The differential reaction calorimeter (Fig. 11.1) was coupled with a hydrogen volumetric measurement, allowing simultaneous thermodynamic and kinetic studies of the reaction. In a typical experiment the "sample" vessel was filled with the reactants and the "reference" cell with the solvent (NaOH solution). The oil circulating in the jackets maintains the surroundings of the reactor at a constant temperature. The used calorimeter principle is based on the continuous measurement of the temperature difference between the two vessels during the experiment. In order to determine the heat capacity (Cp) of the system and correlate the temperature difference (ΔT) to the heat flow, a Joule-effect calibration is performed before and after each reaction step (see Fig. 11.2), and the corresponding energy is obtained by the $Q = Cp \times \Delta T$ equation. The measured heat corresponds to the global energy evolved during the $NaBH_4$ hydrolysis reaction after each addition of fresh reactants ($NaBH_4$ solution stabilized by NaOH) (Fig. 11.2). The endothermic effects observed at the beginning of each peak correspond to the addition of the reactive solution at a temperature slightly lower than that of the thermostated vessel. In their paper [43] the authors show that the total enthalpy of the catalytic process is strongly influenced by the evolution of the catalyst during the hydrolysis reaction and by some water evaporation which is related to the $NaBH_4$ concentration. For the first time the calorimetric
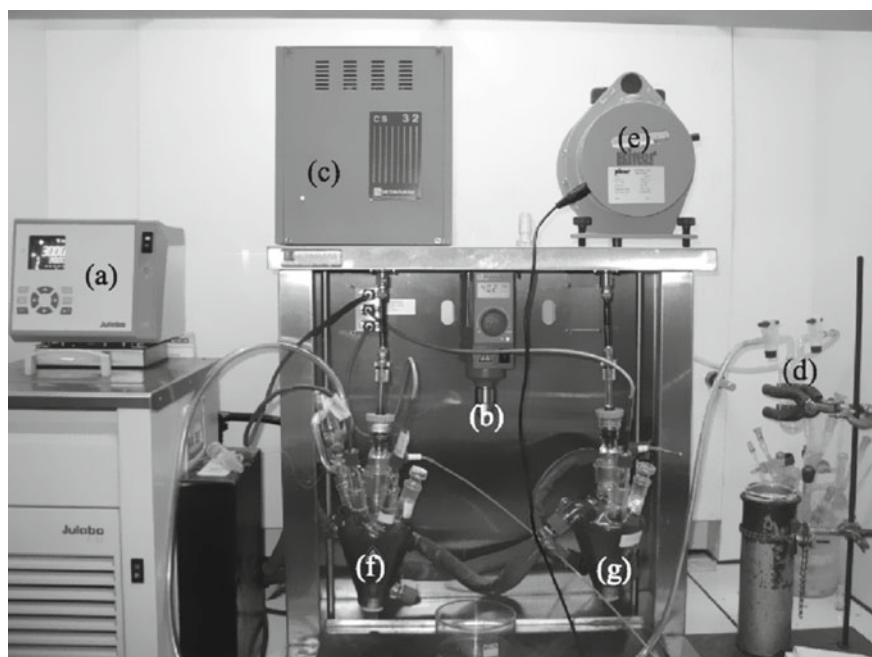

Fig. 11.1 Picture of the DRC system coupled with a volumetric gas-meter. **a** Julabo Thermostat. **b** IKA parallel stirrers. **c** DRC CS 32 control unit. **d** liquid N_2 trap. **e** Gas volume-meter Ritter TG01. **f** measurement cell. **g** reference cell
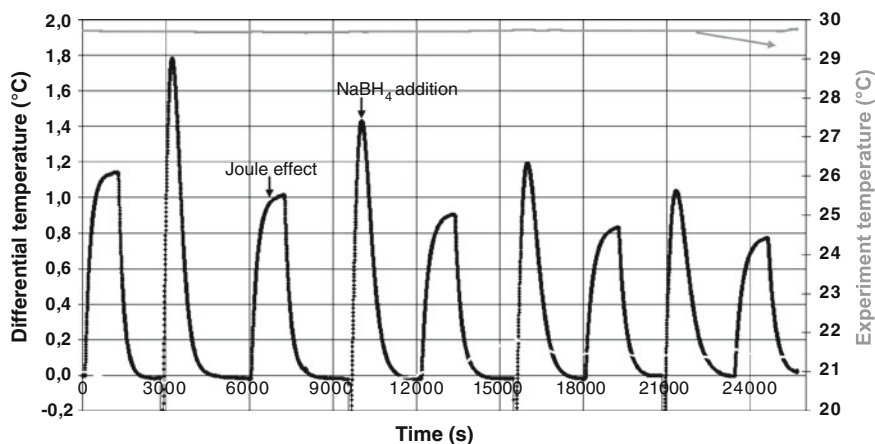
Fig. 11.2 Typical profile of a DRC analysis with 4 injections (10 mL) of NaOH-stabilized solution of $NaBH_4$ (19 wt.%) on 1 mmol Co-nanoparticles suspended in 20 mL water. Before and after each injection peak a Joule effect is performed for determining the relative heat of reaction
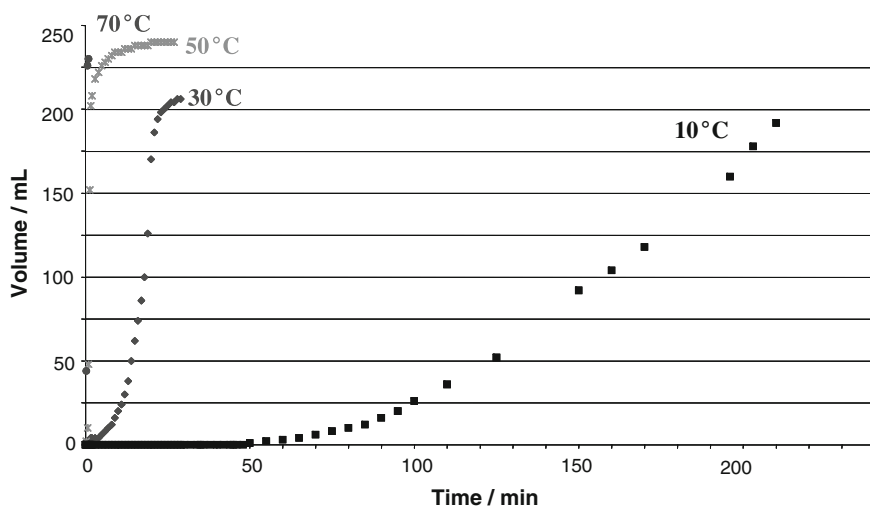

Fig. 11.3 Evolution versus time of the hydrogen generation at different temperatures for the $NaBH_4$ hydrolysis reaction (Injection of 0.2 mL of water on a solid mixture of 200 mg $NaBH_4$ + 20 mg of $Co(H_2O)_6Cl_2$

technique was used to study the catalytic reaction in aqueous phase as complement of "ex situ" characterization of the solid catalyst and the reacting solution, thus providing "operando" information about the reaction thermodynamics and kinetics and consequently the mechanism.

The setup shown in Fig. 11.1 was thermostated so that experiments reported in Fig. 11.3 could be performed at constant temperature between $-5\,°C$ and $70\,°C$, with
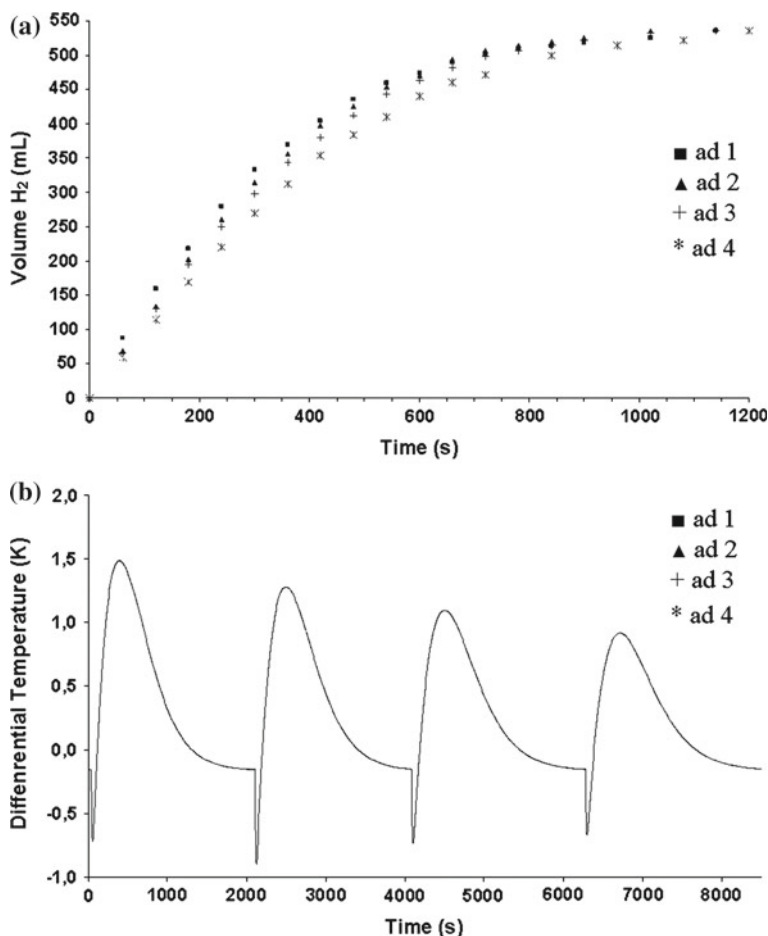
Fig. 11.4 Evolution versus time of the hydrogen generation (**a**) and of the differential temperature (**b**) for the four successive additions of 10 mL of a NaOH-stabilized solution of sodium borohydride (2 wt% $NaBH_4$ stabilized by 5.7 mmol NaOH) at 30 °C on the in situ generated catalyst (1 mmol $Co(H_2O)_6Cl_2$ + 20 mL of H_2O + 5 mmol $NaBH_4$ dissolved in 5 mL of H_2O)

the purpose of determining the activation energy by studying the dependence of the rate of hydrogen production on the temperature. The activation energy determined in this manner was -42.7 kJ.mol^{-1} [43].

Figure 11.4 shows the evolution of the hydrogen volume and differential temperature *versus* time upon four successive additions of $NaBH_4$ solution (Fig. 11.4a, b). The curves of the amounts of evolved hydrogen (Fig. 11.4a) for each addition show similar profiles, with a kinetic response that slightly decreases with each successive addition as the concentration of metaborate and the total volume of the reactant solution increase. In fact, the presence of residual sodium metaborate

during the reaction lowers the ability of borohydride to reach the catalyst surface [43, 44]. The four differential temperature peaks obtained after successive additions of solution (Fig. 11.4b) present very similar shapes, but the increasing of the width at half-height (thermokinetic parameter), confirmed that thermal transfer within the solution becomes increasingly difficult as its viscosity increases (Fig. 11.4b). Nonetheless, the total area of the peak, and hence the total energy evolved during the reaction, remain constant.

The activity towards $NaBH_4$ hydrolysis of metals which can be readily oxidized and form stable boride species was also studied by liquid reaction calorimetry [45]. Co, Ni, and Fe are stable in alkaline aqueous media and they are not affected by the concentration of residual metaborate in the solution. In Ref. [45] the use of liquid-phase calorimetric methods provided deep insight on the catalytic behaviour of the samples by studying the energy production and its evolution as a function of time. The volume of hydrogen generated at a given time is reported in Fig. 11.5 for Co, Ni and Fe salts acting as catalysts in the $NaBH_4$ hydrolysis reaction.
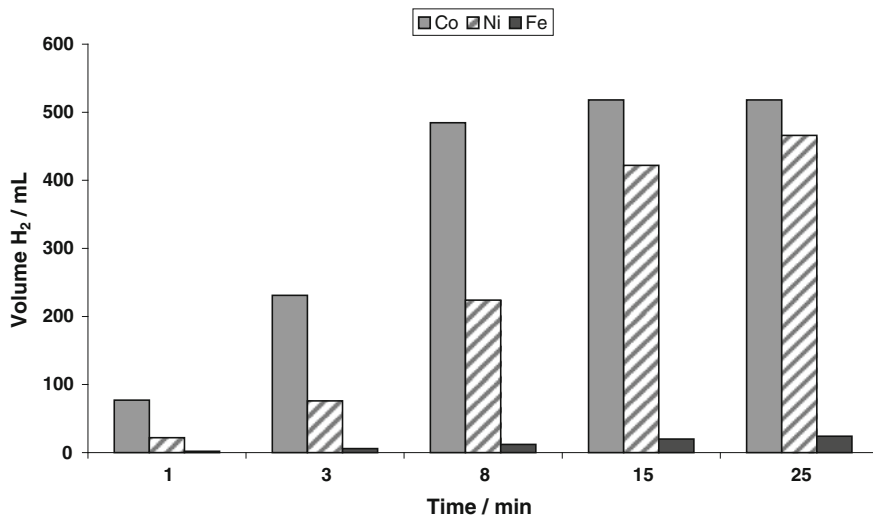

Fig. 11.5 Hydrogen volumes generated at 1, 3, 8, 15, and 25 min for Co, Ni and Fe salts acting as catalysts. Catalyst generated in situ by addition of 5 mL of aqueous solution containing 200 mg of $NaBH_4$ on the chloride salt (1 mmol equivalent of metal in 20 mL water), pH = 14 by addition of 5 mL NaOH 6 M. Test: additions of 10 mL of $NaBH_4$ (2 wt.% solution) stabilized by 10 mmol of NaOH (4 wt.%) [45]

11.2.2 *Hydrolysis of* NaBH₄ *and* KBH₄ *Powders*

The hydrogen storage capacity of sodium borohydride depends on the quantity of water involved in the whole storage system. For example, for a standard commercial solution containing 20 wt% of $NaBH_4$ the storage capacity corresponds to 4.2 wt% H_2. Higher hydrogen storage capacities can be achieved by the reaction of stoichiometric quantity of water with solid sodium borohydride. If the water content in the $Na,KBH_4(s)/catalyst(s)/H_2O(l)$ system is high enough to dissolve the metaborate product at room temperature (25 °C), the advantages of this configuration are the possibility to store the reagents separately and to remove the products of the reaction from the system in liquid form, avoiding the formation of a borate solid crust that will decrease the diffusion of water in the solid reactants [46].

To mimic and study this storage configuration the instrument used was a Calvet type differential heat flow microcalorimeter which allows continuous stirring of liquid-solid mixtures (Fig. 11.6). After stabilization of the calorimeter baseline, the water (or the hydrolyzing solution) was added to the sample cell which contains the potassium or sodium borohydride powders (eventually activated with a catalyst) and to the empty reference cell in the same way using a programmable twin syringe pump linked to the calorimeter by capillary tubes. The reaction cell had a home-made airtight cap with attached inox outlet tubing. The inox tube was linked to a gas volume meter allowing continuous measurement of generated hydrogen.

Because hydrolysis of $NaBH_4$ and KBH_4 is a very slow process and the rate of hydrogen generation from this reaction depends on the addition of a catalyst and on
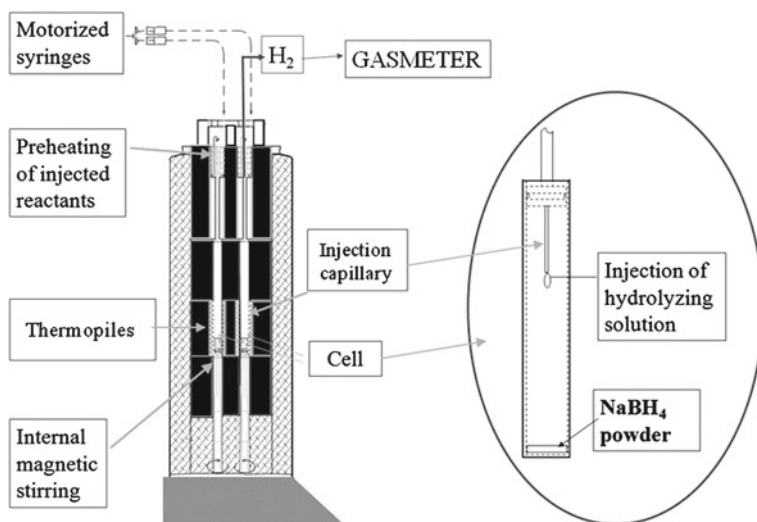

Fig. 11.6 Scheme of the Titrys calorimeter coupled with a volumetric gas-meter and a programmable twin syringe pump

its preparation method, the study of non-catalyzed hydrolysis can be very difficult as well as the experimental determination of the reaction heat. In fact, long time scale experiments are challenging in terms of accuracy of the total evolved heat (integral method) determination.

Self-hydrolysis occurs spontaneously but slowly when $NaBH_4$ and KBH_4 are in contact with water, and liquid calorimetry coupled with a gas-meter (Fig. 11.6) permits to precisely determine the heats of the hydrolysis reaction for $NaBH_4$ and KBH_4 that are respectively of -236 and $-220 \, kJmol_{Na,KBH4}^{-1}$ [46]. These values were obtained by integration of the calorimetric peaks shown in Fig. 11.7 that display the heat flow evolved during the hydrolysis reactions of $NaBH_4$ and KBH_4 without catalyst. The endothermic signal visible on the heat flow signal versus time curves for both investigated borohydrides is attributed to the water injection. The hydrolysis reaction is an exothermic process and, after an initial increase, the heat flow signal reaches an almost constant value until the end of the hydrolysis reaction, when it exhibits an abrupt decrease. The value of the measured heat includes the enthalpy of dissolution of the borohydride, the enthalpy of the hydrolysis reaction, the enthalpy of dissolution of the by-product ($NaBO_2$ or KBO_2) and the evaporation of some water during the exothermic reaction.

Therefore, to increase the decomposition rate of $NaBH_4$ by hydrolysis a catalyst is needed. As already pointed out, cobalt-based catalysts have shown promising activity, and acids are also suitable catalytic accelerators [47, 48].

In Fig. 11.8 the heat flow peaks for the $NaBH_4$ hydrolysis reaction in presence of malic acid (a), Co-nanoparticules (b) and pure water (c) are reported, and the heats of reaction obtained by integration of these peaks were respectively of -298, -244, and $-236 \, kJ \cdot mol_{NaBH4}^{-1}$. By analyzing the shape of the calorimetric peaks a perception of the hydrogen release kinetics can be obtained; the most rapid
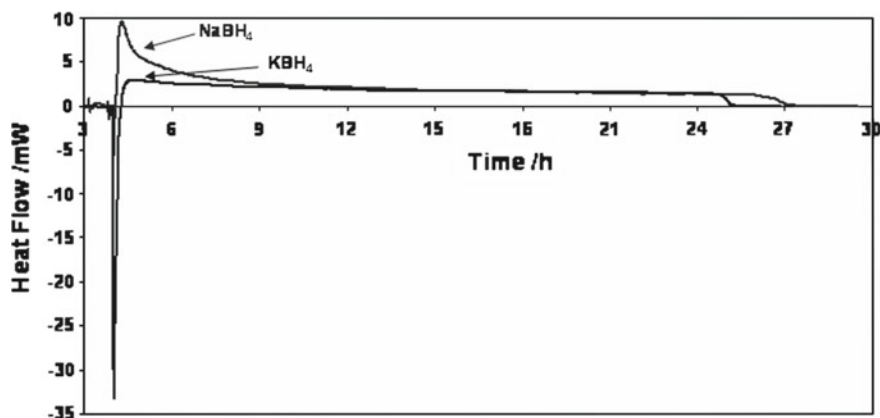

Fig. 11.7 Heat flow signals versus time for $NaBH_4$ and KBH_4 hydrolysis without catalyst (1 mL water on 30 mg borohydride)
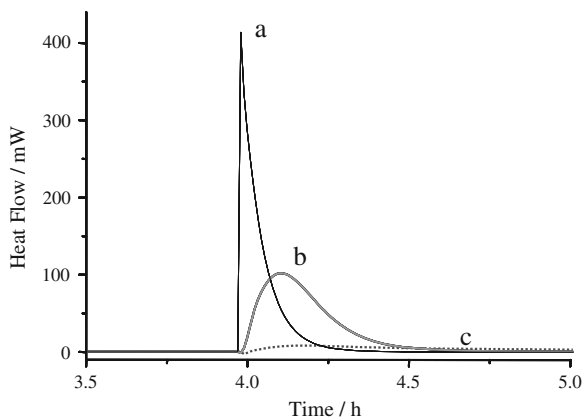
Fig. 11.8 Heat flow generated during $NaBH_4$ hydrolysis by addition of **a** 1 mL of 1 M maleic acid, **b** 1 mmol Co-nanoparticules dispersed in 1 mL of water, and **c** pure water
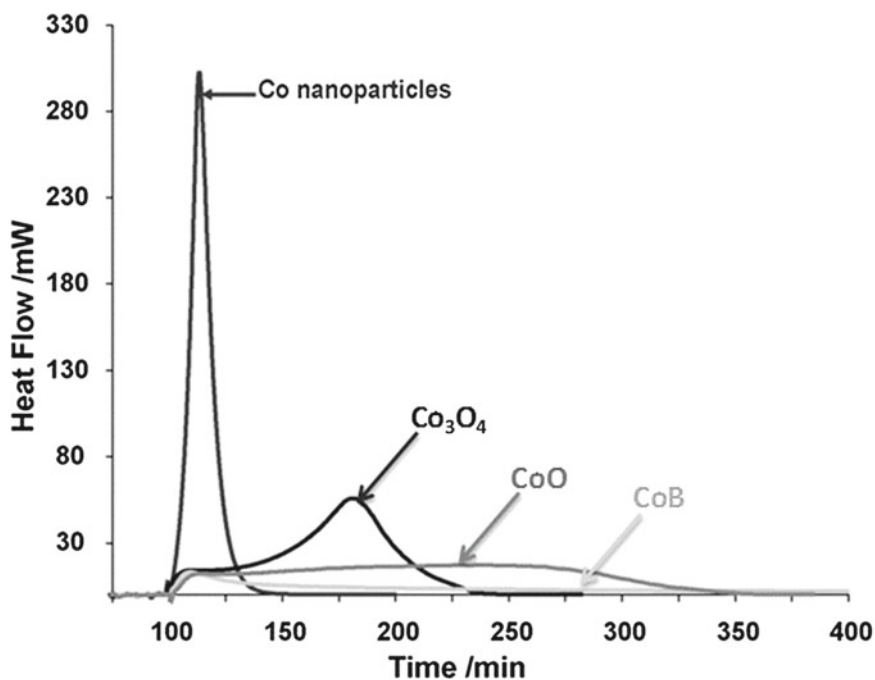

Fig. 11.9 Heat flow signals versus time for KBH_4 hydrolysis reaction in the presence of different Co-based solids (30 mg of KBH_4 and an amount of catalyst equivalent to 10 wt% of pure Co)

hydrogen production corresponds to the use of malic acid and it can be noticed that the faster reaction corresponds to the higher heat generated.

The experimental calorimetric curves obtained for the hydrolysis reaction of $NaBH_4$ in the presence of different catalysts (Co nanoparticles, CoO and Co_3O_4) are shown in Fig. 11.9, as well as the curve obtained for the $NaBH_4$ hydrolysis reaction without catalyst reported as reference. The measured heats of the $NaBH_4$ hydrolysis reaction were -243, -235, and $-236\,kJ \cdot mol^{-1}_{NaBH4}$ in the presence of Co nanoparticles, CoO, and Co_3O_4, respectively [46]. The reaction times for the complete hydrogen generation were: 33 min for Co nanoparticles, 120 min for Co_3O_4 and 240 min for CoO. In all cases, 100 % of the stoichiometric amount of hydrogen was generated during the stated reaction time [46]. Much higher hydrogen production rates ($6000\,mL\,min^{-1}g_{Co}$, corresponding to a reaction time of 7 min) were measured in the same way on Co based catalysts with the cobalt phase dispersed on acidic heteropolyanions supports [49].

By means of liquid calorimetry coupled with a volumetric gas-meter Damjanovic et al. [50] have shown that addition of solid NaOH to the reacting mixture ($NaBH_4$ + catalyst) increases the rate of $NaBH_4$ hydrolysis reaction in the presence of Co-based catalysts. Comparing the results available in the literature it is clear that the effect of NaOH concentration on the hydrolysis generation rate greatly depends on the type of catalysts [51]. Consequently, it is important to find an optimum range for NaOH concentration to improve the hydrogen generation rate in the presence of Co based catalysts. Figure 11.10 shows the experimental calorimetric curves obtained for hydrolysis of 30 mg of $NaBH_4$ in the presence of 4.1 mg of Co_3O_4 (corresponding to 10 wt% of pure Co with respect to sodium borohydride), and different amounts of solid NaOH. The measured heats after injection of 0.5 ml of water were
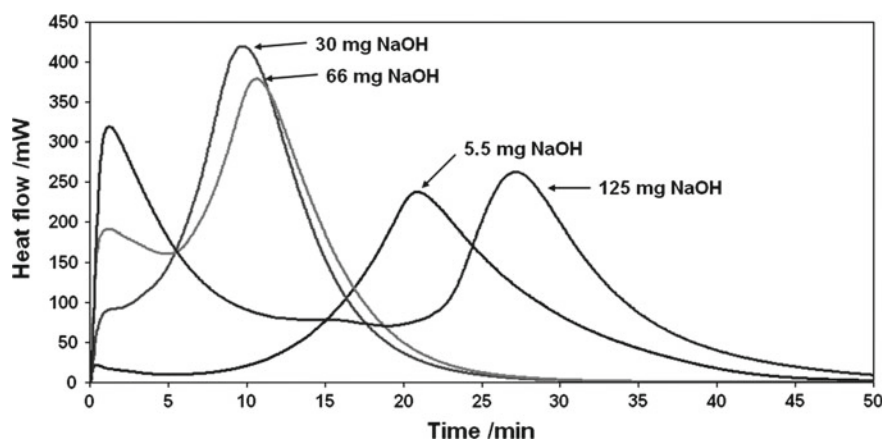

Fig. 11.10 Heat flow signals versus time for injection of 0.5 mL of water on 30 mg of $NaBH_4$ hydrolysis in the presence of 4.1 mg of Co_3O_4, and different amounts of solid NaOH (as reported on the figure)

-225, -420, -390 and $-250\,\mathrm{kJmol^{-1}}$ for 5.5, 30, 66 and 125 mg of solid NaOH, respectively [52]. As it can be seen on Fig. 11.5, a clear shift from 20 to about 10 min of the peak maximum occurs when increasing the amount of solid NaOH added from 5.5 to 30 mg. Adding a balanced amount of solid NaOH (around 15–20 mg) to the "NaBH$_4$ + catalyst" mixture improves the kinetics of the reaction and creates a real benefit in terms of reaction kinetics. In parallel to the calorimetry measurements, the volume of generated H$_2$ versus time during the NaBH$_4$ hydrolysis reaction in the presence of Co$_3$O$_4$, and different amounts of solid NaOH was determined. Full conversion was achieved after 35, 12, 15 and 40 min for 5.5, 30, 66 and 125 mg of solid NaOH, respectively. The maximum rates reached over Co$_3$O$_4$ were 8, 16, 16 and 10 ml min^{-1} for 5.5, 30, 66 and 125 mg of solid NaOH, respectively, as presented in Fig. 11.11 [50].

Another experimental solution is to inject very small amounts of water (that will act as limiting reactant) and to avoid any separation step involving reactants and reacted products. In this simpler configuration the issues to solve are the improvement of the water diffusion in the solid (once the first injection performed and consequently further NaBO$_2$ · xH$_2$O formed) and the optimisation of water consumption (by reducing the NaBO$_2$ hydration ratio).

To give an answer to these issues, interesting studies about the thermal properties of NaBH$_4$ solid mixtures were obtained with other thermal techniques, as reported in Ref. [16], where an infrared camera has been used to evaluate the temperature
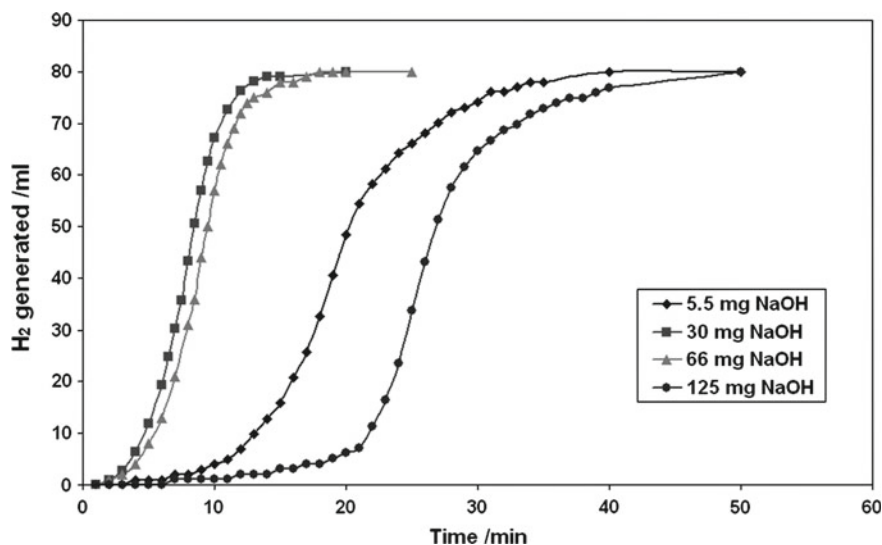

Fig. 11.11 Evolution versus time of the hydrogen generation for injection of 0.5 mL of water on 30 mg of NaBH$_4$ in the presence of 4.1 mg of Co$_3$O$_4$, and different amounts of solid NaOH (as reported on the figure)
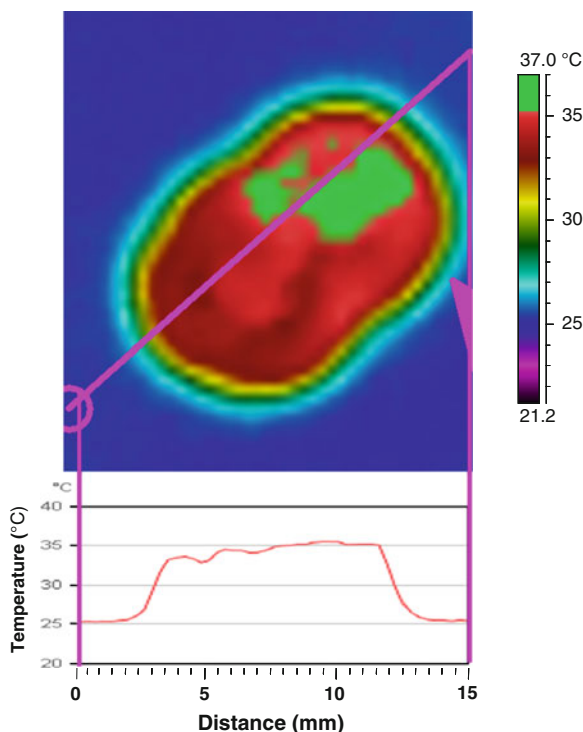
Fig. 11.12 Thermal imaging and temperature profile during the hydrolysis of $NaBH_4 + 10\,wt\%$ nCo at $25\,°C$ in presence of a less-than-stoichiometric amount of water

profile in a $NaBH_4 +$ Co-nanoparticles solid mixture (with or without addition of solid NaOH) when a drop of water is added (Fig. 11.12).

Knowing that the major limitation to reach the theoretical $10.9\,wt\%$ H_2 storage density by hydrolysis of $NaBH_4$ powder with water is the hydration level of the metaborate product, to attain a higher H_2 storage density, a higher temperature of the system is required for dehydrating the metaborate products, and an easy way to reach this objective is to utilize the thermal effects of hydrolysis.

These thermal effects associated to the hydrolysis reaction have been studied on a fully dehydrated $NaBH_4$ powder by means of an IR imaging camera and a differential titration calorimeter. Various amounts of solid sodium hydroxide were added to the system ($NaBH_4 +$ metallic nanoCobalt catalyst) allowing an increase of the maximum reaction temperature (up to $140\,°C$). The reaction maximum temperature and the hydrogen yield were considerably modified by varying the amount of NaOH and the amount of catalyst (Fig. 11.13). At a temperature of more than $140\,°C$, it is reasonable to expect the formation of low hydration borate phases. In fact, at temperatures above $105\,°C$ water is expected to participate preferentially in the hydrolysis reaction rather than in the hydration of the
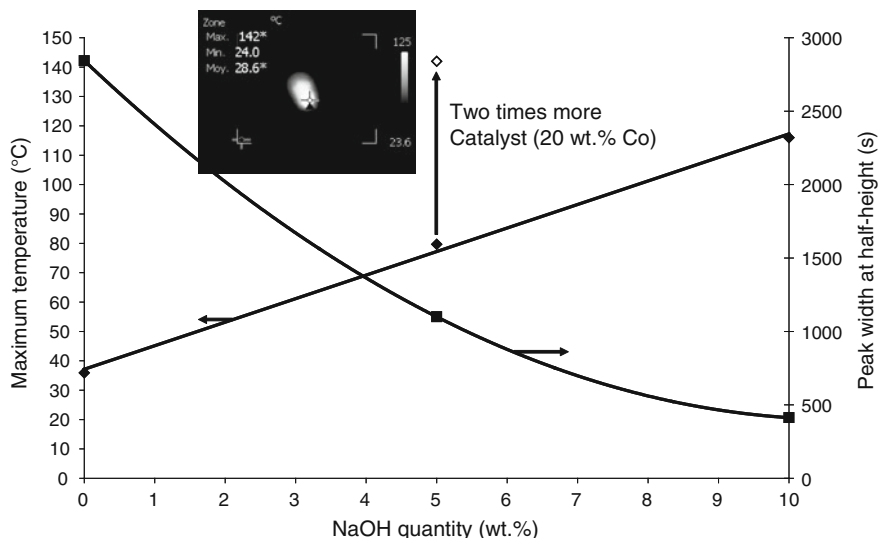
Fig. 11.13 Maximum temperature (*left side*) and peak width at half-height (*right side*) as functions of the sodium hydroxide loading, and comparison with the results obtained with twice the amount of catalyst (the two curves are obtained in presence of 10 wt% nCo catalyst)

formed metaborate [52]. Moreover the absence of highly hydrated borate favors the diffusion of water by avoiding the formation of the hydrophobic $NaBO_2 \cdot 2H_2O$ layer.

11.3 Second Case Study: Reversible H_2 Storage (Mg-Based Materials)

As mentioned in the introductory section of this chapter, for automotive applications the requirements for on-board hydrogen storage are very severe, as mainly stated by the United States Department of Energy [7] and the Japanese Government. The same kind of restrictions are also associated to the storage of intermittent energies where the amount of energy involved can be extremely high and consequently a stable storage system is required. To reach the demanded targets for the application in the automotive field research efforts have been made to develop interstitial, binary or even more complex hydrides capable to store and release hydrogen at temperature and pressure compatible with the different applications. For example, Mg (non toxic and inexpensive) shows a hydrogen storage capacity of 7.7 wt%, but the major impediment is its high H_2 desorption temperature (>300 °C). In order to decrease the desorption temperature of MgH_2 many research groups have tried to add other hydrides to MgH_2 in order to form complex hydrides with lower hydrogen desorption
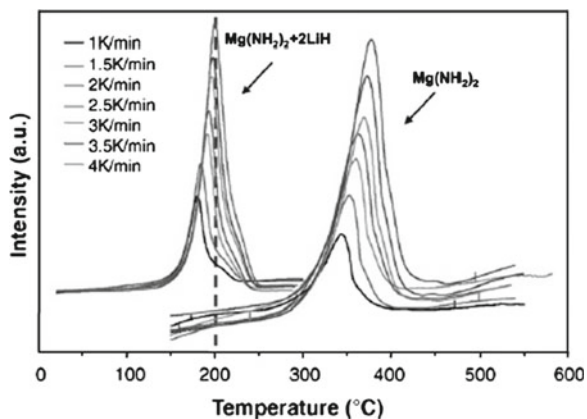
Fig. 11.14 DSC profiles for $(Mg(NH_2)_2 + 2LiH)$ and $Mg(NH_2)_2$ at various scan rates [30]

temperature. Temperature programmed desorption techniques (TPD, DSC, TG) are the right tools to follow the hydrogen desorption process, determining the desorption temperature, evaluating the amount of desorbed H_2 and in DSC measuring the heat associated to the hydrogen release.

As example, the Li-Mg-N-H system was studied by differential scanning calorimetry by Gross's group [53]. The major issue for metal-N-H storage systems is the formation of NH_3, that takes place in parallel with H_2 release, and that acts as a
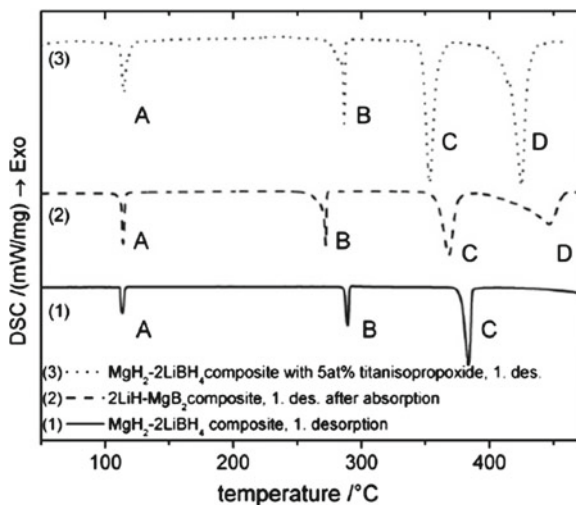

Fig. 11.15 HP-DSC of the desorption reaction of $MgH_2–2LiBH_4$ composites after milling (*1*), after initial hydrogenation (*2*) and after milling with additive (*3*). Heating rate $5°C \cdot min^{-1}$; 20 $mL_{H2} \cdot min^{-1}$; 3 bar H_2 [57]
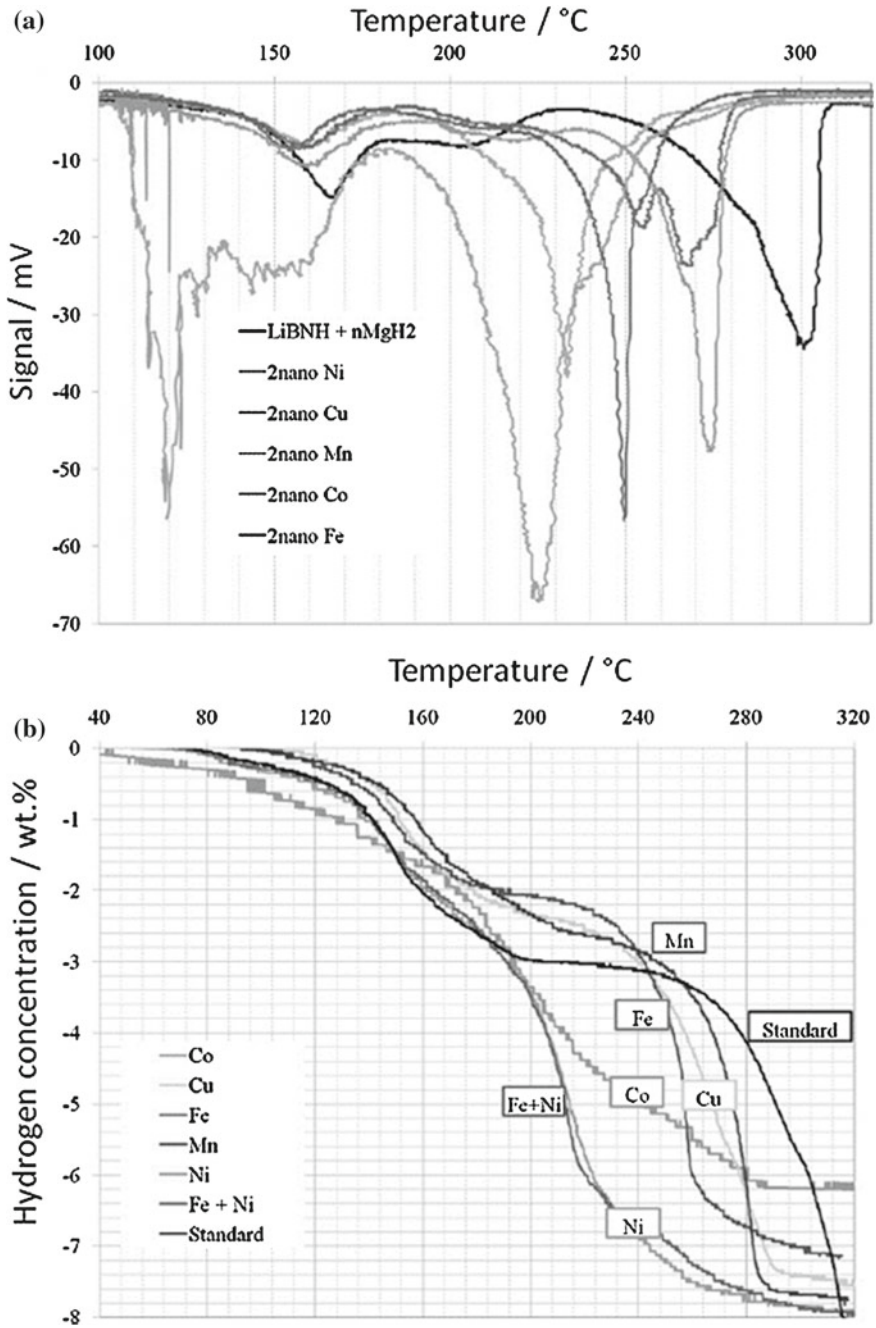
Fig. 11.16 a TPD comparison of LiBNH + nMgH$_2$ without additive and with 2 mol% Ni, Cu, Mn, Co and Fe at a constant ramping rate of 1°C/min and **b** Ramping kinetics measurements of LiBNH + nMgH$_2$ without and with 2 mol% nano Mn, Fe, Co, Cu, Ni and Fe + Ni [24]
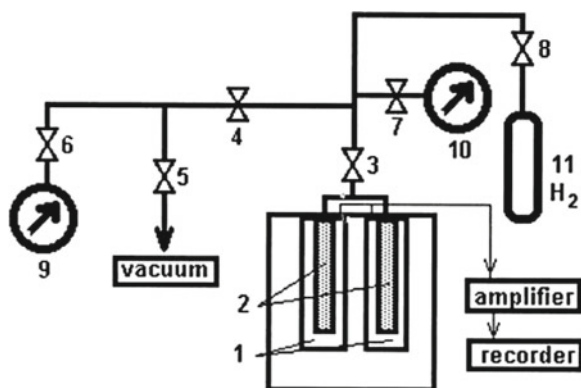
Fig. 11.17 Scheme of the calorimetric device: (*1*) calorimetric chambers; (*2*) calorimetric cells (reaction and blank); (*3–8*) needle valves; (*9*) vacuum gauge; (*10*) pressure gauge; (*11*) hydrogen source

poison for the PEM fuel cell catalysts [54]. As reported in Fig. 11.14, the lower temperature peak obtained by DSC method and centered at 200 °C is related to hydrogen release by the $Mg(NH_2)_2 + 2LiH \rightarrow Li_2Mg(NH_2)_2 + H_2$ reaction, while the higher temperature peak corresponds to the self-decomposition of Mg amide (irreversible reaction) related to NH_3 production. The identification of these phenomena and of their relative temperatures helps to identify the maximum working temperature necessary to avoid the $Mg(NH_2)_2$ decomposition and improve the cyclic stability of the material.

Addition of $LiBH_4$ to Mg allows to decrease the hydrogen desorption temperature by approximately 30 °C by formation of MgB_2 intermediary species [55, 56]. New techniques as high-pressure differential scanning calorimetry (HP-DSC) have been used to verify the mechanism of decomposition of MgH_2–$LiBH_4$ composites as well as the influence of the addition of different additives such as titanium isopropoxide and VCl_3, under 3 bar hydrogen pressure [57]. As shown in Fig. 11.15, the absorption-desorption cycling and the addition of additives deeply influence the kinetics of hydrogen release. As consequence, the peaks C and D shift at lower temperature for the MgH_2–$LiBH_4$ materials activated by the absorption reaction (curve 2) or by addition of titanium isopropoxide (curve 3).

Novel complex hydrides ($LiBH_4$/$LiNH_2$/MgH_2) are also under study and the addition of various nanosized additives as nickel, cobalt, iron, copper, manganese was followed by thermoprogrammed desorption technique (TPD) [24].

The TPD tool was used in Ref. [24] to identify the optimal hydrogen release temperature and to get an indication of the H_2 desorption rate by measuring the peak width. In Fig. 11.16, the addition of the different additives has a big effect on reducing the temperature of the second H_2 releasing peak.

Unusual are set-ups combining Tian-Calvet calorimetry and high pressure volumetric lines. One of the few examples is reported in the work of Anikina and Verbetsky

in Ref. [58]: the schematic diagram of their set-up is reported on Fig. 11.17. This technique was used to study TiZrMnV compounds used as H_2 storage system. Desorption molar enthalpies were determined and used in support to the researcher assumption that the material was composed of two different hydride phases, $Ti_{0.9}Zr_{0.1}Mn_{1.1}H_{1.0}$ and $Ti_{0.9}Zr_{0.1}Mn_{1.1}H_{2.0}$, respectively at low and high hydrogen content.

11.4 Conclusions

Different kinds of hydrogen storage materials have been studied and reported in the recent literature, but only few candidates are able to answer to the requirements for portable and on-board applications. The main problems still to be solved are the continuous control of the reaction for safety reasons, the increasing of the kinetics of hydrogen release, and the reversibility of the reaction to perform adsorption/desorption cycling.

For an extensive use of these materials it is important to deeply understand the thermal phenomena associated to hydrogen release reactions and adsorption/desorption cycles.

The thermodynamic features of these systems (enthalpies, entropies) as well as the thermal properties of the involved compounds (thermal conductivity, heat capacity) are crucial data to predict the thermal behavior of large quantity of material, as those used in real applications.

Calorimetry and thermal analysis techniques (alone or coupled to other instruments) have been developed and applied to the study of hydrogen storage systems. As example, information about the heat evolved during the hydrogen release as a function of time has given the possibility to contemporarily evaluate the kinetics of reaction and to point out the presence of diffusion problems, connected to borohydride hydrolysis. In other showcases the identification of specific thermal phenomena helped in understanding the reaction mechanism and the material structure.

It is certain that calorimetry and thermal analysis are indispensable tools in the study of hydrogen storage and further developments and applications of these techniques have to be expected in the near future.

References

1. G. Marban, T. Valdes-Solis, Int. J. Hydrogen Energy **32**, 1625 (2007)
2. D.A.J. Rand, R.M. Dell, *Hydrogen Energy* (The Royal Society of Chemistry, Cambridge, 2008)
3. F. Jackow, J. Loughead, European Technology Platform for Hydrogen and Fuel Cells (HFP), Implementation plan-status 2006 http://www.fch-ju.eu/sites/default/files/documents/hfp-ip06-final-apr2007.pdf/
4. L. Schlappbach, A. Züttel, Nature **414**, 353 (2001)
5. B. Sakintuna, F. Lamari-Darkrimb, M. Hirscher, Int. J. Hydrogen Energy **32**, 1121 (2007)
6. S.F.J. Flipsen, J. Power Sour. **162**, 927 (2006)

7. U.S. Department of Energy Hydrogen Program, http://www.hydrogen.energy.gov/
8. U.B. Demirci, O. Akdim, P. Miele, Int. J. Hydrogen Energy **34**, 2638 (2009)
9. S. Bakker, Int. J. Hydrogen Energy **35**, 6784 (2010)
10. C. Cakanyildirim, M. Guru, Int. J. Hydrogen Energy **33**, 4634 (2008)
11. S.U. Jeong, R.K. Kim, E.A. Chob, H.-J. Kim, S.-W. Nam, I.-H. Oh, S.-A. Hong, S.H. Kim, J. Power Sour. **144**, 129 (2005)
12. B.H. Liu, Z.P. Li, J. Power Sour. **187**, 527 (2009)
13. S.C. Amendola, S.L. Sharp-Goldman, M.S. Janjua, N.C. Spencer, M.T. Kelly, P.J. Petillo, Int. J. Hydrogen Energy **25**, 969 (2000)
14. Y. Kojima, K.I. Suzuki, K. Fukumoto, M. Sasaki, T. Yamamoto, Y. Hawai, Int. J. Hydrogen Energy **27**, 1029 (2002)
15. J.S. Zhang, W.N. Delgass, T.S. Fisher, J.P. Gore, J. Power Sour. **164**, 772 (2007)
16. S. Bennici, A. Garron, A. Auroux, Int. J. Hydrogen Energy **35**, 8621 (2010)
17. B.H. Liu, Z.P. Li, S. Suda, J. Alloys Compd. **415**, 288 (2006)
18. P. Krishnan, K.L. Hsueh, S.D. Yim, Appl. Catal. B **77**, 206 (2007)
19. R. Chen, X. Wang, L. Xu, L. Chen, S. Li, C. Chen, Mater. Chem. Phys. **124**, 83 (2010)
20. A. Züttel, P. Sudan, P. Mauron, P. Wenger, Mater. Sci. Eng. B **108**, 9 (2004)
21. N. Eigen, F. Gosch, M. Dornheim, T. Klassen, R. Bormann, J. Alloys Compds. **465**, 310 (2008)
22. M. Ismail, Y. Zhao, X.B. Yu, S.X. Dou, Int. J. Hydrogen Energy **35**, 2361 (2010)
23. K.R. Graham, T. Kemmitt, M.E. Bowden, Energy Environ. Sci. **2**, 706 (2009)
24. S.S. Srinivasan, M.U. Niemann, J.R. Hattrick-Simpers, K. McGrath, P.C. Sharma, D.Y. Goswami, E.K. Stefanakos, Int. J. Hydrogen Energy **35**, 9646 (2010)
25. P. Chen, Z. Xion, J. Luo, J. Lin, K.L. Tan, Nature **420**, 302 (2002)
26. W.N. Yang, C.X. Shang, Z.X. Guo, Int. J. Hydrogen Energy **35**, 4534 (2010)
27. C.X. Shang, Z.X. Guo, Int. J. Hydrogen Energy **32**, 2920 (2007)
28. D. Dybtsev, C. Serre, B. Schmitz, B. Panella, M. Hirscher, M. Latroche, P.L. Llewellyn, S. Cordier, Y. Molard, M. Haouas, F. Taulelle, G. Férey, Langmuir **26**, 11283 (2010)
29. M. Latroche, S. Suble, C. Serre, C. Mellot-Draznieks, P.L. Llewellyn, J.-H. Lee, J.-S. Chang, S.H. Jhung, G. Ferey, Angew. Chemie Int. Ed. **45**, 8227 (2006)
30. H.W. Langmi, D. Book, A. Walton, S.R. Johnson, M.M. Al-Mamouri, J.D. Speight, P.P. Edwards, I.R. Harris, P.A. Anderson, J. Alloys Compds. **637**, 404 (2005)
31. G.E. Ioannatos, X.E. Verykios, Int. J. Hydrogen Energy **35**, 622 (2010)
32. V.G. Minkina, S.I. Shabunya, V.I. Kalinin, V.V. Martynenko, A.L. Smirnova, Int J. Hydrogen Energy **33**, 5629 (2008)
33. D.R. Lide, *CRC Handbook of Chemistry and Physics*, 82nd edn. (CRC Press, Boca Raton, 2001)
34. A. Stock, *Hydrides of Boron and Silicon* (Cornell University Press, Ithaca, 1933)
35. J.C. Ingersoll, N. Mani, J.C. Thenmozhiyal, A. Muthaiah, J. Power Sour. **173**, 450 (2007)
36. J. Zhang, T.S. Fisher, J.P. Gore, D. Hazra, P.V. Ramachandran, Int. J. Hydrogen Energy **31**, 2292 (2006)
37. N.O. Gonzales, M.E. Levin, L.W. Zimmerman, J. Hazard. Mater. **142**, 369 (2007)
38. J. Li, B. Li, S. Gao, Phys. Chem. Miner. **27**, 342 (2000)
39. S. Bennici, A. Auroux, Thermal Analysis and Calorimetric Methods, in *Metal Oxide Catalysis*, vol. 1, ed. by S.D. Jackson, S.J. Hargreaves (Wiley-VCH Verlag GmbH & Co, Weinheim, 2009), p. 391
40. H. Nogent, X. Le Tacon, L. Vincent, N. Sbirrazzuoli, J. Loss Prev. Process Ind. **18**, 43 (2005)
41. R. Andre, L. Bou-Diab, P. Lerena, F. Stoessel, M. Giordano, C. Mathonat, Organ. Process Res. Dev. **6**, 915 (2002)
42. J. Andrieux, D. Swierczynski, L. Laversenne, A. Garron, S. Bennici, C. Goutaudier, P. Miele, A. Auroux, B. Bonnetot, Int. J. Hydrogen Energy **34**, 938 (2009)
43. A. Garron, D. Swierczynski, S. Bennici, A. Auroux, Int. J. Hydrogen Energy **34**, 1185 (2009)
44. S.J. Kim, J. Lee, K.Y. Kong, C.R. Jung, I.G. Min, S.-Y. Lee, H.-J. Kima, S.W. Nam, T.-H. Lim, J. Power Sour. **170**, 412 (2007)
45. A. Garron, S. Bennici, A. Auroux, Appl. Catal. A **378**, 90 (2010)

46. L. Damjanovic, S. Bennici, A. Auroux, J. Power Sour. **195**, 3284 (2010)
47. O. Akdim, U.B. Demirci, P. Miele, Int. J. Hydrogen Energy **34**, 4780 (2009)
48. H.I. Schlesinger, H.C. Brown, A.E. Finholt, J.R. Gilbreath, H.R. Hoekstra, E.K. Hyde, J. Am. Chem. Soc. **75**, 215 (1953)
49. S. Bennici, H. Yu, E. Obeid, A. Auroux, Int. J. Hydrogen Energy **36**, 7431 (2011)
50. L. Damjanovic, S. Bennici, A. Auroux, Int. J. Hydrogen Energy **36**, 1991 (2011)
51. H. Tian, Q. Guo, D. Xu, J. Power Sour. **195**, 2136 (2010)
52. E.Y. Marrero-Alfonso, J.R. Gray, T.A. Davis, M.A. Matthews, Int. J. Hydrogen Energy **32**, 4723 (2007)
53. W. Luo, J. Wang, K. Steward, M. Clift, K. Gross, J. Alloys Compds. **336**, 446 (2007)
54. G. Postole, A. Auroux, Int. J. Hydrogen Energy **36**, 6817 (2011)
55. S. Orimo, Y. Nakamori, G. Kitahara, K. Miwa, A. Ninomiya, H. Li, N. Ohba, S. Towata, A. Zuttel, J. Alloys Compd. **427**, 404 (2005)
56. J.J. Vajo, S.L. Skeith, F. Mertens, J. Phys. Chem. B Lett. **109**, 3719 (2005)
57. U. Bosenberg, S. Doppiu, L. Mosegaard, G. Barkhordarian, N. Eigen, A. Borgschulte, T.R. Jensen, Y. Cerenius, O. Gutfleisch, T. Klassen, M. Dornheim, R. Bormann, Acta Materialia **55**, 3951 (2007)
58. E.Yu. Anikina, V.N. Verbetsky, J. Alloys Compd. **45**, 330 (2002)